

# Parametric Analysis on the Lateral Force Resistance of Qing Dynasty Timber Frame Containing Stacked Purlins

Yibin Chang <sup>a,b</sup> and Jian Dai <sup>a,b,\*</sup>

In ancient wooden structures of the Qing dynasty in China, stacked purlins are important longitudinal elements. In this study, a refined finite element model of a four-column timber frame containing stacked purlins was built. The effects of the fangs, spacer boards, and purlins with dovetail ends on the lateral resistance of the timber frame and the mid-span vertical deflection of the purlins were studied. The longitudinal hysteresis curve of the timber frame made up of stacked purlins was found to be S-shaped, centrally symmetrical, with a pinching effect and full at both ends. The Fangs made the greatest improvement on the lateral stiffness, displacement ductility, and total hysteresis energy consumption of the timber frame by reducing the mid-span vertical deflection of the purlins. The spacer boards contributed less to the lateral resistance of the timber frame than Fangs, but they contributed most to the reduction of the mid-span vertical deflection of the purlins. The dovetail connection at the ends of the purlins had a limited effect on reducing the lateral stiffness and ductility of the timber frame and increasing the mid-span vertical deflection of the purlins, but they significantly increased the total energy consumption of the timber frame and its energy consumption capacity.

DOI: 10.15376/biores.18.3.4723-4738

*Keywords:* Traditional Chinese timber frame; Stacked purlins; Lateral force resistance; Hysteretic behavior

*Contact information:* a: Faculty of Architecture, Civil and Transportation Engineering, Beijing University of Technology, Beijing 100124, China; b: Key Science Research Base of Safety Assessment and Disaster Mitigation for Traditional Timber Structure (Beijing University of Technology), State Administration for Cultural Heritage, Beijing 100124, China; \*Corresponding author: [ibin1009@126.com](mailto:ibin1009@126.com)

## INTRODUCTION

Traditional Chinese architecture is based on wooden structures and has developed over thousands of years, with each dynasty developing its own unique style in terms of architectural forms and structural systems. In the twelfth year of the Yongzheng reign (1734) of the Qing dynasty, the official book *Engineering Practice* was issued, in which the regulations on the form and dimensions of building structures were made more standard and concise. Stacked purlins, recorded in the book, are found in the remains of ancient wooden structures of the Qing dynasty as an important component of longitudinal connections (Fig. 1). The stacked purlin is composed of three parts: purlin, spacer board, and fang. The upper part of the purlin supports the roof, and the lower two ends are connected to the beam. Below the purlin is the spacer board, and below the spacer board is the fang. Stacked purlins are generally found at the ridge, at the eaves of timber-framed buildings without dou-gong bracket (Fig. 2), and in the section between the eaves and the ridge. The stacked purlins bear the roof structure vertically and connects each bay of the frame horizontally. Together with the timber frame of the columns, the stacked purlins contribute to lateral and longitudinal resistances.



(a) The Guandi Temple at the Temple of Ancient Monarchs



(b) The gates of Prince Gong's Palace



(c) The Fasting Palace at the Temple of Heaven



(d) The Jingyun Gate of the Forbidden City

**Fig. 1.** Stacked purlins in Qing dynasty timber-framed ancient buildings. 1. Purlin; 2. Spacer board; 3. Fang

There are some studies on the mechanical properties of timber frames in four-column spaces of ancient buildings. Wang *et al.* (2021) developed a refined finite element model of a four-column timber frame from the Tang dynasty and investigated the effects of the dou-gong layer, the position and magnitude of the column head and footings, and the vertical loads on the hysteretic energy dissipation and lateral force resistance performance of the timber frame by means of proposed static numerical simulation tests. Seismic time-history analyses of this timber frame were used to investigate the seismic performance of the structure and the energy dissipation characteristics of the structural layers (Wang *et al.* 2022). Chen *et al.* (2018) and Meng *et al.* (2019) conducted a proposed static test study on the Song-style single-room four-column timber frame model, revealing its seismic mechanism and the effect of loading history on its hysteretic energy dissipation and lateral stiffness resistance. Sun *et al.* (2022) investigated the kinematic mechanism of a 1/16 scale four-post pavilion-type timber frame under seismic excitation by shaking table tests. Several typical states of motion during the kinematic deformation of the timber frame were described, and a finite element model was developed to predict the dynamic response of the timber frame. Chen (2016) investigated the force performance of single-bay beam-raising and Chuan-dou timber frames of the Qing Dynasty based on theoretical analysis, finite element simulation and model test methods, respectively. In Japan, Fujita (2019)

carried out shaker tests on four different types of bracket complexes. The results were compared with those obtained by static lateral loading tests, and the validity of a proposed structural model was discussed. Maeno *et al.* (2004) conducted a simulated static and shaking Table test study on a Japanese four-column traditional building model and concluded that the restoring force of such timber frames is provided by the resisting moment of the crossbeams and the restoring force generated by the sway of the columns.

Stacked purlins or stacked beams are found in traditional Chinese timber-frame buildings. Wu *et al.* (2020) established a stacked beam containing Pupai fang using the Yingxian wooden pagoda of the Liao dynasty as a reference prototype, and obtained parameters such as hysteresis curves by means of a proposed static lateral resistance test method and proposed a simplified load-displacement model with three-line segments. Han *et al.* (2021) investigated the effect of the number and position of nails on the bending moment, slip, deflection, and ultimate load carrying capacity of Qing dynasty stacked purlins by means of a three-point bending test method. Sun *et al.* (2020) used a stacked purlin in a Qing dynasty ridge part as a model and measured the moment-angle hysteresis curve through a proposed static test to analyse the force-deformation characteristics and damage modes of the node. Zhou and Yang (2016) summarised the common damage conditions of the stacked purlins of ancient buildings in the Forbidden City with regard to their structural composition and force characteristics. They analysed the causes of the problems and made recommendations for strengthening. Han and Chun (2016) carried out a mechanical analysis based on the bolt fitting method in traditional timber building restoration, using the bolt fitting three-frame beam model, the bolt fitting five-frame beam model, and the bolt fitting purlin model, and compared them using ANSYS finite element software. Cao *et al.* (2015) investigated the mechanical properties of double-layered stacked beams in ancient Tibetan wooden structures through mechanical analysis and proposed a non-linear analytical model for double-layered stacked purlins. Zhou and Yan (2012) used mechanical analysis to study the vertical bending stresses of stacked and combined purlins in timber structures of ancient buildings.

Most research of the timber structure of ancient buildings has focused on the vertical bending performance of the stacked purlins or stacked beams, but there has not been much research on the lateral resistance of the wood frame composed of it and the columns. In particular, there has been little research on the lateral resistance of this typical form of stacked purlins consisting of purlin, spacer board, and fang in Qing dynasty timber structures. Currently, research on the mechanical properties of traditional timber frames, particularly in the joints and connections, is relatively common and mature using finite element methods. Examples include studies on dovetail or straight mortise and tenon joints (Li *et al.* 2020; Pan *et al.* 2020, 2021), as well as complex traditional timber frames with two-column (Wan *et al.* 2020) or four-column (Chen 2017) formats. These simulation results have shown high agreement with experimental tests. Therefore, referring to these finite element simulation methods similar to the mortise and tenon joints and timber frames of this research object, a four-column timber frame containing stacked purlins was established according to the *Engineering Practice*, and its lateral resistance was investigated by pseudo-static testing with finite element software. The effect of the spacer board, Fang, and purlins with dovetail ends on the lateral resistance performance was investigated.

## MATERIALS AND METHODS

### Construction of Stacked Purlins in Qing Dynasty Timber Frame

The distribution of stacked purlins in a typical Qing dynasty timber-framed building is shown in Fig. 2. The composition and dimensions of the members of the laminated purlin are shown in Fig. 3. The uppermost layer is the purlins, which are connected by dovetails and placed in half-round recesses on either side of the beam ends. The spacer board are placed immediately below the purlins, and the ends are inserted in rectangular recesses on either side of the beam end. The beams rest directly on the top surface of the columns, and they are connected to each other by means of Mantou-tenons. The fang is similar to a square beam, with its ends made into dovetails, connected to the mortise on either side of the column above, and the upper part of it fitting snugly into the spacer board.

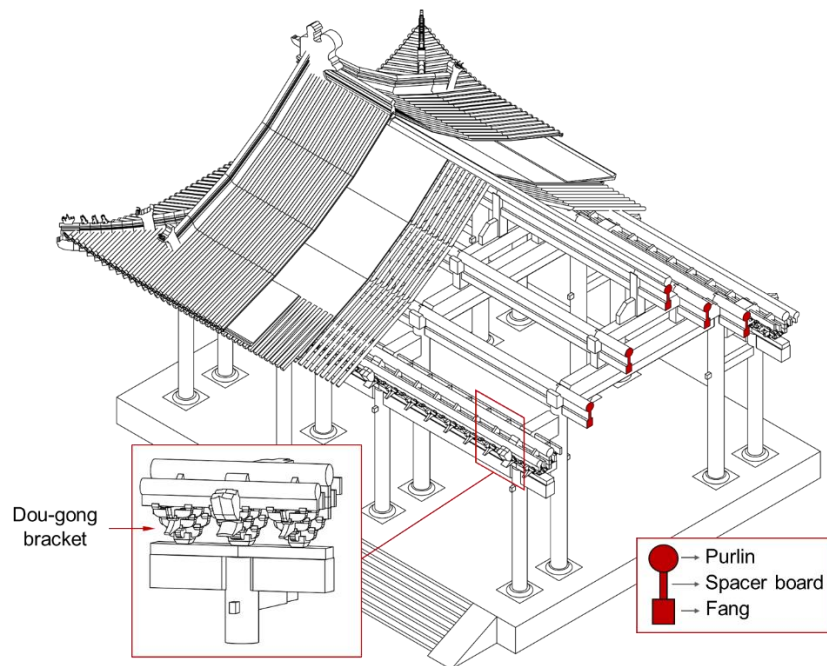


**Fig. 2.** Stacked purlin in a typical Qing dynasty timber frame

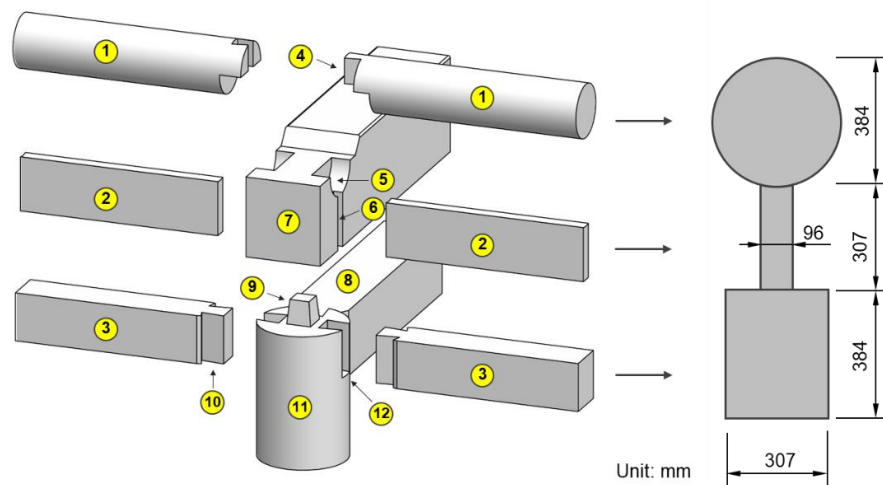


**Fig. 3.** Construction and dimensions of stacked purlins. 1. Purlin; 2. Spacer board; 3. Fang; 4. Dovetail; 5. Half-round Recess; 6. Square Recess; 7. Beam; 8. Follow Beam-Fang; 9. Mantou-Tenon; 10. Dovetail; 11. Column; 12. Mortise.

### Dimensions of Finite Element Model

A refined finite element model LDF-1 of a four-column timber frame was built based on the dimensional provisions of the *Engineering Practice*. The dimensions of the mortises and tenons and the detailed construction of the joints between them were referred to in the *Construction Technology of Ancient Chinese Architecture* (Ma 2003). The timber frame is made up of stacked purlin in the longitudinal direction and five-purlins beam and follow beam-Fang in the transverse direction. The roof frame and roof sections were converted into loads applied to the five-purlin beams and eaves purlins. Three additional groups of models LDF-2, LDF-3 and LDF-4 were produced as controls to investigate the effect of the member's performance against lateral forces. LDF-2 has no spacer board, LDF-3 has no fang, and the ends of LDF-4 purlins are made into dovetails. The finite element model for the four groups of timber frames is shown in Fig. 4. The dimensions of each member in the model are shown in Table 1. The horizontal low circumferential cyclic load test was simulated using the finite element software ABAQUS. The 8-node hexahedral linearly reduced integral solid unit C3D8R was used as a solid finite unit. The members are connected by mortise and tenon. The action between the components was set by "contact", and the normal action was simulated by "hard contact"; the tangential friction was selected as Coulomb friction type. The friction coefficient was 0.4 (Xie *et al.* 2018).

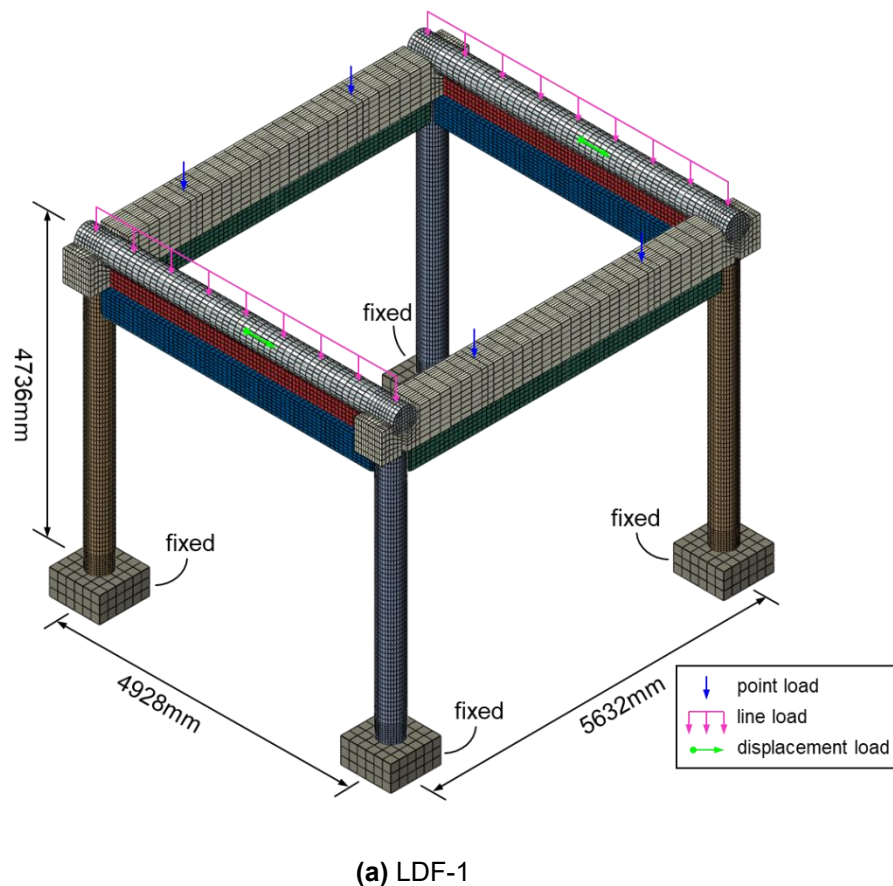


Fig. 4(a). Refinement finite element mode

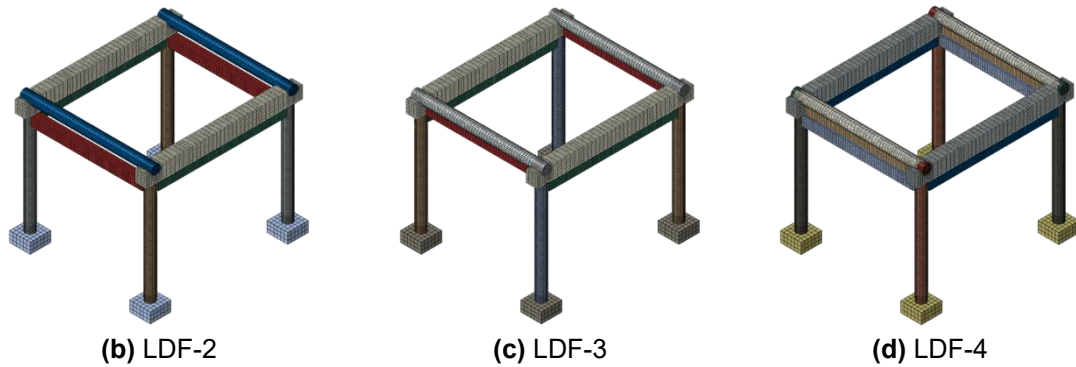


Fig. 4(b-d). Refinement finite element mode

Table 1. Dimensions of Components

Components	Height (mm)	Thickness (mm)	Length (mm)
Eave purlin	384.0	384.0	4928.0
Five-purlin beam	576.0	460.8	6016.0
Eave spacer plate	307.2	96.0	4582.4
Follow beam-Fang	384.0	307.2	5478.4
Eave Fang	384.0	307.2	4774.4
Eaves column	384.0	384.0	4224.0
Pedestal	422.4	844.8	844.8

### Material Parameters

In this study, Mongolian Scots pine (*Pinus sylvestris* var. *mongolica*) was used as the model timber for two reasons: firstly, Mongolian Scots Pine is an important fast-growing timber species in northeastern China, with strong material, straight texture, strong adaptability, and excellent resistance to adversity, making it a good building material and often used as timber for ancient buildings in the north. Secondly, many universities and research units are also currently using Mongolian Scots pine as a test material for timber frame ancient buildings. For this reason, Mongolian Scots pine has also been a common choice of material in previous numerical simulation studies of timber-framed ancient buildings. In finite element software simulations, wood is generally modelled using an orthogonal anisotropic intrinsic model. The mechanical property parameters of the Mongolian Scots pine (Li 2015) are shown in Table 2. The pedestal was made of granite with a modulus of elasticity of 55000 MPa, Poisson's ratio of 0.2 and a density of 2800 kg/m<sup>3</sup>.

Table 2. Material Property Parameters of Mongolian Scots Pine

Elastic Modulus (MPa)			Poisson's Ratio			Shear Modulus (MPa)			Density kg/m <sup>3</sup>
$E_L$	$E_R$	$E_T$	$U_{RL}$	$U_{TL}$	$U_{TR}$	$G_{LR}$	$G_{RT}$	$G_{LT}$	$\rho$
3805	268	154	0.5	0.1	0.35	268	154	268	460

Note:  $E$  is the elastic modulus;  $U$  is Poisson's ratio;  $G$  is the shear modulus; L, R, and T refer to the longitudinal, radial, and tangential directions respectively;  $\rho$  is the density.

## Roofing Load

In accordance with the official traditional timber roof construction practice (Liu 2001a,b), the roof layers from top to bottom are the barrel-tiles, gray lime-back, white lime-back, straw clay-back, board-guard lime, wang-board, and rafters. In Table 3, the weight of each layer of material for the roof was counted. An equivalent surface load of 7.12 kN/m<sup>2</sup> was calculated for the roof covering.

**Table 3.** Calculation of Roof Load

Layered Construction	Thickness (cm)	Mass (kg/m <sup>2</sup> )	Weight (kN/m <sup>2</sup> )
Barrel-tiles	-	264	2.59
Gray lime-back	3	51	0.50
White lime-back	3	51	0.50
Straw clay-back	8	160	1.57
Board-guard lime	1.5	32	0.31
Rafter with Wang- board		133	1.30
Snow load			0.35
Grand total			7.12

## Loading Scheme

A horizontal low circumferential cyclic displacement was applied to the middle of the purlin, as shown in Fig. 4a. The displacement was increased at a rate of  $\pm 25$  mm to a maximum amplitude of  $\pm 250$  mm for a total of 10 cycles. The exact loading scheme is shown in Fig. 5.

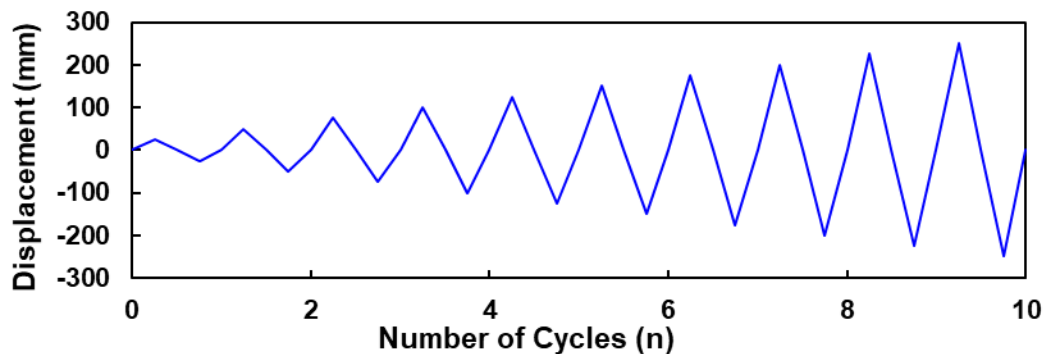


**Fig. 5.** Loading process of the test

## RESULTS AND DISCUSSION

### Deformation Characteristics

When a longitudinal horizontal low circumferential cyclic displacement was applied, the LDF-1 swayed from side to side. Figure 6a shows the stress cloud for LDF-1 at the maximum forward horizontal displacement. During forward loading, the purlin translated in the direction of loading and created slip friction with the lower spacer board. The dovetail on the right-hand side of the purlin rotated against the half-round recess of the five-purlin beam. The five-purlin beam on the left had no relative displacement or rotation to the column head, while the one on the right rotated against the column and rubbed against the tenons in the column head. The spacer board between the two beams also translated with the timber frame, creating slip friction with the lower fang. As the fang

moved horizontally, it also rotated relative to the column, which in turn caused the dovetails at its ends to squeeze and rub against the mortise at the top of the column. In the horizontal reciprocating movement of the stacked purlin, frictional slippage occurred between the members, and they fit more closely in the vertical direction. The left side of the bottom surface of the column gradually rose and separated from the top surface of the pedestal, while the right side and the top surface of the pedestal squeezed each other. There was little relative slip in the horizontal direction between the column and the pedestal. After the horizontal displacement had been loaded, plastic deformation occurred mainly in the lower part of the dovetail of the Fang and at the junction of the column mortise, as well as on the sides of the column base along the longitudinal direction. As shown in Fig. 6b, 6c, 6d, and 6e, the plastic deformation of the dovetails at the ends of the Fang is 0.012, the plastic deformation of the tenons on the head of the column is 0.022 and the plastic deformation of the base of the column is 0.031.

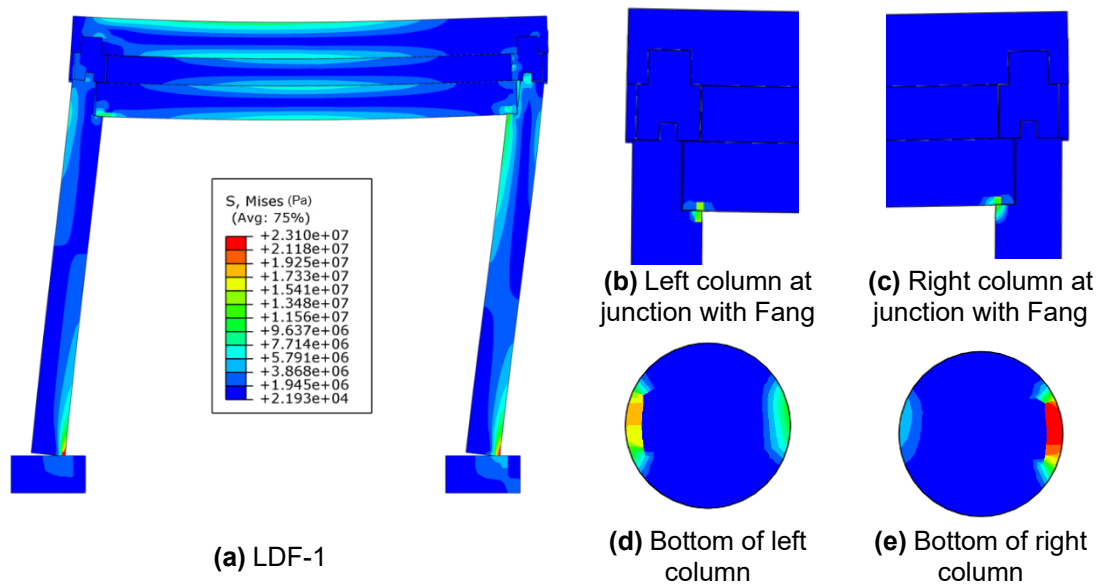


Fig. 6. Stress cloud of LDF-1 and plasticity cloud of key areas

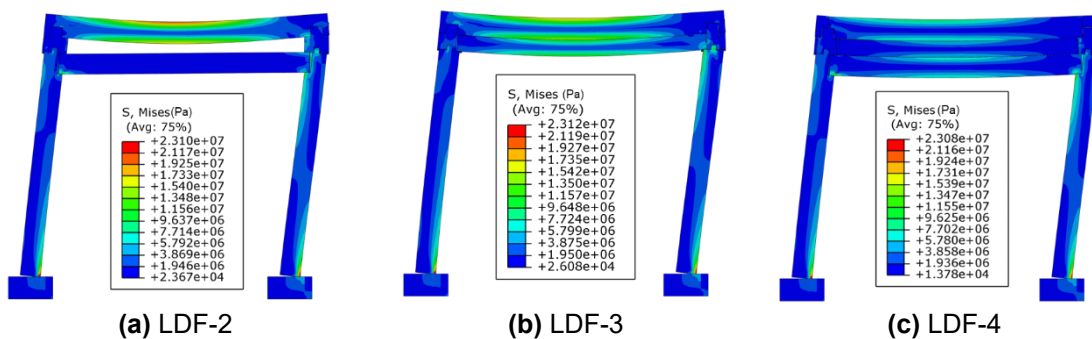


Fig. 7. Stress cloud of LDF-2, LDF-3, and LDF-4

As shown in Fig. 7, the deformation characteristics of LDF-2, LDF-3, and LDF-4 are essentially similar to those of LDF-1. Due to the lack of spacer board in LDF-2, the lower part of the purlin was unsupported and caused excessive vertical deflection, resulting in plastic deformation of the half-round recess on the inner side of the five-purlin beam at

the beginning of loading. After loading, the dovetail of the fang showed pull-out, with an overall pull-out of 14.1 mm. LDF-3 was missing the fang, and thus the vertical deflection of the purlin and spacer board was also excessive. The lower part of the spacer board ends were plastically deformed due to extrusion and friction. In LDF-4, the two ends of the purlins were dovetailed, and the dovetails split and closed with each other as the model swayed from side to side during the loading process. The purlins and the half-round recesses of the five-purlin beam also split and squeezed each other, resulting in a large slip friction with the spacer board.

### Hysteresis Curve

Figure 8 shows the hysteresis curves for the four groups of models, which are approximately centrosymmetric. LDF-1, LDF-2, and LDF-3 are S-shaped, and LDF-4 is shuttle-shaped. The hysteresis curves increased almost linearly at the beginning of loading, and the hysteresis loop area was small, indicating that the structure is in an elastic state at this stage. As the horizontal displacement increased, the horizontal thrust increased non-linearly and the area of the hysteresis loop increased. After reaching the peak, the horizontal thrust gradually decreased. All four sets of curves exhibited a pinching effect. Compared to LDF-1, LDF-2 had a significant pinching and a reduced hysteresis loop area. This was due to the lack of a spacer board in LDF-2, which reduced some of the friction and increases the slip between the components. The LDF-3 had a smaller hysteresis loop than all three of the others, which was caused by the lack of Fang members. The dovetail ends of the LDF-4 purlins increased the friction between the purlins and the spacer board and between the purlins and the half-round recess, resulting in a fuller hysteresis curve.

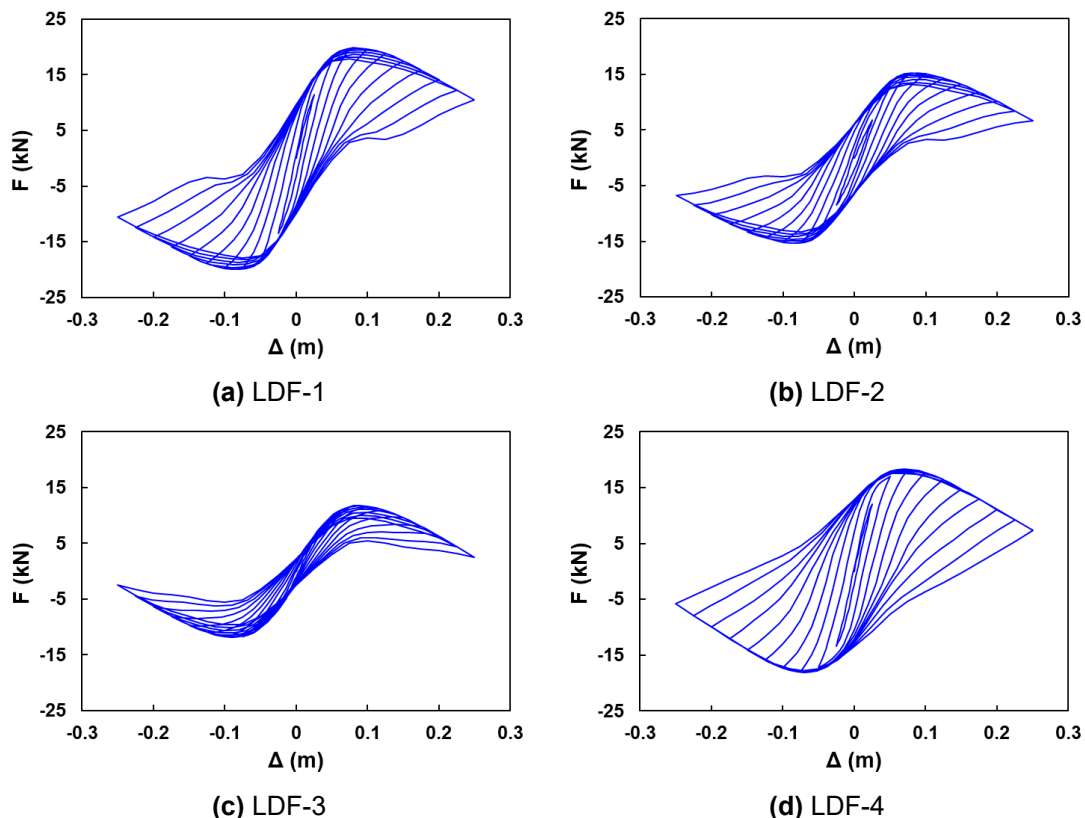


Fig. 8. Hysteresis curves

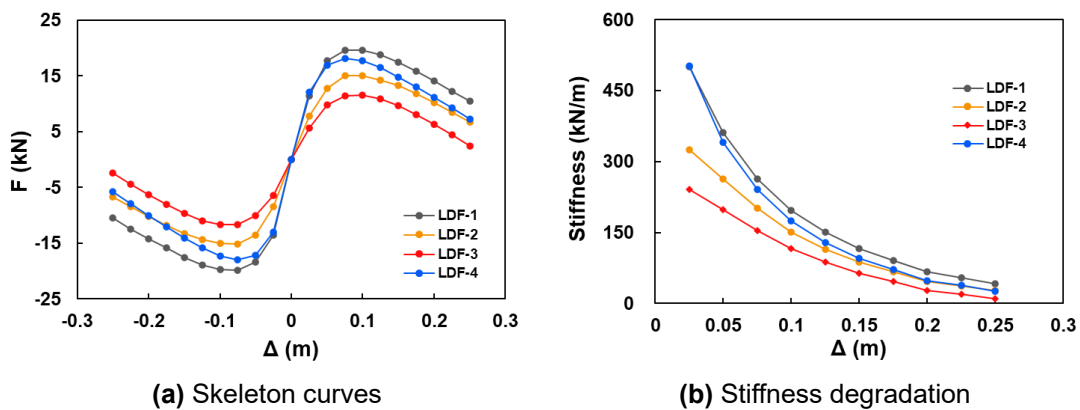
**Lateral Force Resistance and Ductility**

Figure 9a shows the skeleton curves for the four sets of models, which follow approximately the same trend. With the exception of model LDF-4, which intersected LDF-2 at a stage where the negative loading distance  $\Delta > 0.2$  m, the absolute magnitude of the thrusts for the remaining four curves were LDF-1 > LDF-4 > LDF-2 > LDF-3.

As the model skeleton curve has no obvious yield point, the yield point of the skeleton curve was therefore determined using the generic yield moment method (Feng *et al.* 2017). The displacement corresponding to the drop in peak load to 80% was taken as the damage point. The displacement ductility factor, which is the ratio of the deformation of the structure at failure to the deformation at yield, can be used to assess the deformation capacity of the model under horizontal low circumferential cyclic loading and can be calculated by Eq. 1,

$$\mu = \frac{\Delta_u}{\Delta_y} \tag{1}$$

where  $\Delta_u$  is the deformation at breakage and  $\Delta_y$  is the deformation at yield. Key point parameters such as yield load, peak load, breaking load, and ductility factor for the skeleton curve are shown in Table 4.



**Fig. 9.** Skeleton curves and stiffness degradation curves

**Table 4.** Key Points Parameters

Models	Loading Directions	Yield Point		Peak Point		Breaking Point		Ductility	
		$P_y$ (Kn)	$\Delta_y$ (mm)	$P_p$ (kN)	$\Delta_p$ (mm)	$P_u$ (kN)	$\Delta_u$ (mm)	$\mu$	Avg.
LDF-1	+	17.85	51.3	19.60	75.0	15.68	178.2	3.46	3.72
	-	17.26	44.2	19.82	75.0	15.86	174.1	3.97	
LDF-2	+	13.43	57.2	15.03	75.0	12.02	171.4	3.00	3.09
	-	13.80	53.2	14.22	75.0	12.18	168.5	3.17	
LDF-3	+	10.36	59.1	11.59	100.0	9.27	156.3	2.65	2.74
	-	10.44	54.1	11.69	100.0	9.35	154.5	2.83	
LDF-4	+	16.00	44.1	18.12	75.0	14.50	153.7	3.41	3.54
	-	14.53	40.1	17.95	75.0	14.36	146.5	3.66	

The yield load and peak load of LDF-4 were reduced by 10.2% and 8.5%, respectively, compared to LDF-1. This was due to the dovetail ends of the purlins of LDF-4, which separated between the dovetails during horizontal loading, thus weakening some

of the stiffness. The yield load and peak load of LDF-2 were reduced by 22.5% and 23.3%, respectively, compared to LDF-1. In this model, the spacer board was missing under the purlin, which caused the ends of the purlin to rotate at an angle already under gravity load, resulting in a reduction in stiffness. The absence of spacer boards weakened the integrity of the timber frame, which reduced the lateral stiffness. The yield load and peak load of LDF-3 with the absence of fang were reduced by 40.8% and 41.0% respectively compared to LDF-1, which showed the largest decrease in key point load for this model, indicating that fang is the most important factor affecting the longitudinal lateral stiffness of the model. Compared to LDF-1, the ductility coefficients of LDF-2, LDF-3 and LDF-4 decreased by 17.0%, 26.2% and 4.8% respectively, indicating that the lack of spacers and fang, as well as the dovetail form of the purlin ends, reduced the ductility of the timber frame. The lack of fang had the most significant effect on reducing the deformation capacity of the structure, followed by the lack of spacers and the least effect of dovetail joints at the purlins.

Figure 9b shows the stiffness degradation curves for the four sets of models. Under repeated horizontal loading, the lateral stiffness of the timber frame decreases as the horizontal displacement increases, resulting in stiffness degradation. The lateral stiffness of the structure is expressed as cut-line stiffness and is calculated according to Eq. 2,

$$K_i = \frac{|+P_i| + |-P_i|}{|+\Delta_i| + |-\Delta_i|} \quad (2)$$

where  $i$  is the number of loading cycles;  $K_i$  is the lateral stiffness of the timber frame at the  $i$ -th cycle;  $P_i$  is the peak load at the  $i$ -th cycle; and  $\Delta_i$  is the peak displacement corresponding to  $P_i$ . For LDF-1 and LDF-4, the lateral stiffness degradation was faster when the horizontal displacement  $\Delta \leq 0.1$  m; when the horizontal displacement  $\Delta > 0.1$  m, the stiffness degradation was more moderate. For LDF-2 and LDF-3, the lateral stiffness degradation was more moderate throughout the loading process.

### Energy Consumption Analysis

The area of the hysteresis loop enclosed by each cycle of the hysteresis curve is the energy consumption of one cycle, and the cumulative energy consumption is obtained by accumulating the energy consumption of each cycle.

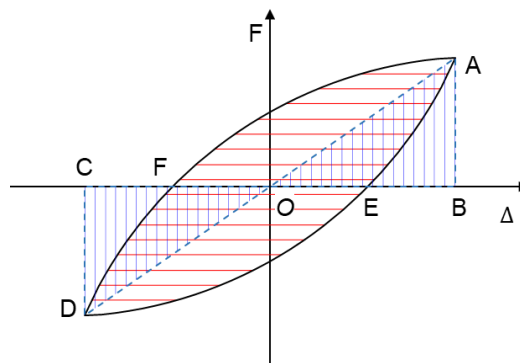


**Fig. 10.** Schematic diagram of the equivalent viscous damping coefficient

In addition to the cumulative energy dissipation, the equivalent viscous damping coefficient  $h_e$  is an important parameter to evaluate the energy dissipation capacity of structures. As shown in Fig. 10, this coefficient is equal to the ratio of the energy dissipated

by the structure in one specific hysteresis cycle over the energy dissipated by its equivalent elastic counterpart when the same deformation is achieved, which is calculated according to Eq. 3.

$$h_e = \frac{S_{AEDF}}{2\pi(S_{\Delta AOB} + S_{\Delta COD})} \quad (3)$$

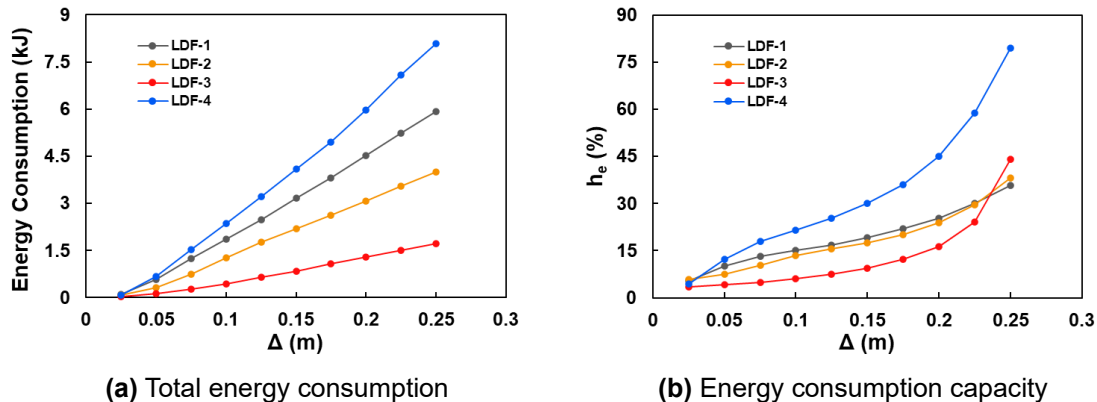


Fig. 11. Total energy consumption and energy consumption capacity

As shown in Fig. 11a, the total energy dissipation-displacement curves for the four groups of models are shown. The energy dissipation was in the order of LDF-4 > LDF-1 > LDF-2 > LDF-3. Compared to LDF-1, LDF-4 had three sections of purlins instead of one complete one. It had a long section in the middle and short sections at the ends, each section was connected to the other by dovetails. This structural form weakened the integrity of the original structure but increased the contact area between the members. Under the application of reciprocal displacement, the model increased the slip friction between the purlins and the spacer board and the half-round recess of the five-purlin beam, thus increasing the overall energy consumption of the model. As there was no spacer board in the LDF-2, there was less friction between the purlins and the spacer board and between the spacer board and the fang, thus reducing the energy dissipation capacity. There was no fang in LDF-3, which not only lacked the friction between the dovetail of the fang and the columns, but also between the fang and the spacer board, so that the total energy consumption of LDF-3 is minimal.

Figure 11b shows the curves of the equivalent viscous damping coefficients with displacement for the four groups of models. At the beginning of loading, the trend of each model curve was similar to the cumulative energy dissipation curve. However, when the absolute value of displacement was greater than 23.75 mm, the equivalent viscous damping coefficient of LDF-3 exceeded that of LDF-1 and LDF-2. This was due to the fact that the rate of increase in the hysteresis area of LDF-3 remained almost unchanged in the later stages of loading, but the lateral force resistance of the structure decreased relatively quickly, resulting in a rapid increase in the coefficient values instead.

### Vertical Deflection

Figure 12 shows the variation of vertical deflection in the purlin span for the four groups of models under the combined effect of gravity and horizontal displacement. The deflection magnitudes are LDF-1 < LDF-4 < LDF-3 < LDF-2.

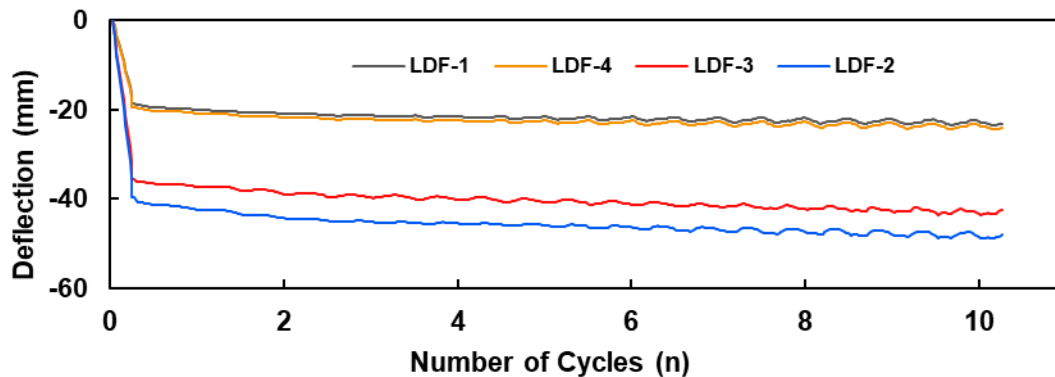


Fig. 12. Deflection as a function of load

The mid-span deflection of the purlin only under the gravity load was  $\omega_1$ , the maximum mid-span deflection of the purlin under the joint action of gravity and horizontal displacement was  $\omega_2$ , and their values are shown in Table 5. According to the *Technical standard for maintenance and strengthening of historic timber buildings* (GB 50165-2020 2020), when the height-to-span ratio is  $h/l > 1/14$ , the vertical deflection limit is calculated as Eq. 4:

$$\omega = \frac{l^2}{2100h} \quad (4)$$

where  $h$  is the height of the beam and  $l$  is the calculated span of the beam, so the limit of deflection of the stacked purlin is 30.1 mm. From the data in Table 5, it can be seen that the deflection in the purlins of LDF-1 and LDF-4 always was able to meet the code requirements no matter under the joint action of gravity or horizontal displacement, while LDF-2 and LDF-3 cannot meet the requirements. Compared to LDF-1,  $\omega_1$  increased by a factor of 1.11 and  $\omega_2$  increased by a factor of 1.08 for LDF-2;  $\omega_1$  increased by a factor of 0.89 and  $\omega_2$  increased by a factor of 0.85 for LDF-3; and  $\omega_1$  increased by a factor of 0.04 and  $\omega_2$  increased by a factor of 0.04 for LDF-4.

Table 5. Deflection Maxima

	LDF-1	LDF-2	LDF-3	LDF-4
$\omega_1$ /mm	18.8	39.7	34.5	19.5
$\omega_2$ /mm	23.5	48.9	43.6	24.5

This indicated that the spacer board made the greatest contribution to reducing the vertical deflection in the purlins, with the fang being the next largest and the dovetail connection in the purlins having the least effect on the deflection. In addition to this, it is easy to see that the horizontal reciprocal displacement increases the deflection in the purlins. This was due to the fact that under horizontal displacement, the model swayed from side to side and the dovetails between the members began to slip or even misalign, resulting in a reduction in the restraint stiffness at both ends of the purlin and thus an increase in the vertical deflection in the purlin span.

## CONCLUSIONS

In this study, a finite element model of a four-column timber frame with stacked purlins was established on the basis of the finite element simulation methods of traditional timber frames and mortise and tenon joints used by previous researchers. The effects of the spacer board, fang, and purlins with dovetail ends on the lateral resistance performance of the timber frame was investigated through pseudo-static simulation tests. Results of this simulation study had it possible to draw the following conclusions:

1. The Qing dynasty four-column timber frame, consisting of stacked purlins, had an S-shaped longitudinal hysteresis curve, was symmetrical in the centre, had a pinching phenomenon, and was full at both ends. The energy in the timber frame was mainly dissipated through frictional slip between the purlins, spacer boards, and fang in the stacked purlins, and between the stacked purlins and the columns and beams. The plastic deformation was mainly concentrated at the junction of the fang and the column, the half-round recess of the purlin and the beam, and at the bottom edge of the column.
2. The dovetail form of the fang ends made the greatest contribution to the lateral stiffness resistance, displacement ductility and total hysteresis energy dissipation of the timber frame. The absence of fang not only reduced the lateral resistance of the timber frame, but also increased the vertical deflection in the purlin span.
3. The spacer board, as a transitional member between the purlins and the fang, contributed less to the lateral resistance of the timber frame than the fang because it is inserted at both ends directly into the beam end and has a smaller cross section than the fang, but it made the greatest contribution to reducing the vertical deflection of the purlins.
4. The dovetail connection at the ends of the purlins weakened the integrity of the timber frame. This reduced the lateral stiffness and ductility of the timber frame to a limited extent and increased the span in the purlins, but it significantly increased the total energy consumption of the timber frame and its energy consumption capacity.

## ACKNOWLEDGMENTS

The study was supported by the National Natural Science Foundation of China (51678005).

## REFERENCES CITED

- Cao, P. L., Yang, Q. S., and Law, S. S. (2015). "Nonlinear analytical model of a two-layer wooden beam in a heritage structure," *Engineering Structures* 101, 494-508. DOI: 10.1016/j.engstruct.2015.07.047
- Chen, C. C. (2016). *Integral Mechanics Property Analysis and Safety Evaluation of Ancient Timber Structures*, Ph.D. Dissertation, Southeast University, Nanjing, China.
- Chen, J. Y. (2017). *Hysteretic Behavior of Full Scale Timber Structure Specimen with Dou-Gong Sets and Four Columns in Song Dynasty by Pseudo-Static Tests and*

- Simulation Analysis*, Ph.D. Dissertation, Taiyuan University of Technology, Taiyuan, China.
- Chen, J. Y., Li, T. Y., Yang, Q. S., Shi, X. W., and Zhao, Y. X. (2018). "Degradation laws of hysteretic behavior for historical timber buildings based on pseudo-static tests," *Engineering Structures* 156, 480-489. DOI: 10.1016/j.engstruct.2017.11.054
- Feng, P., Qiang, H. L., and Ye, L. P. (2017). "Discussion and definition on yield points of materials, members and structures," *Engineering Mechanics* 34, 36-46. DOI: 10.6052/j.issn.1000-4750.2016.03.0192
- Fujita, K. (2019). "Dynamic performance of bracket complexes used in traditional timber structures in Japan," *Proceedings of the Japan Academy, Series B* 95(9), 568-580. DOI: 10.2183/pjab.95.038
- GB 50165-2020 (2020). "Technical standard for maintenance and strengthening of historic timber building," Standardization Administration of China, Beijing, China.
- Han, Y., and Chun, Q. (2016) "Structural mechanism of Chinese traditional timber beams stitched with bolts," *Journal of Nanjing Tech University (Natural Science Edition)* 38(5), 52-60. (in Chinese) DOI: 10.3969 / j.issn.1671-7627.2016.05.009
- Han, X. L., Dai, J., Qian, W., Zhu, Z. Y., and Li, B. L. (2021). "Effects of dowels on the mechanical properties of wooden composite beams in ancient timber structures," *BioResources* 16(4), 6891-6909. DOI: 10.15376/biores.16.4.6891-6909
- Liu, D. K. (2001a). "Load assembler of roofing of ancient building (The first volume)," *Traditional Chinese Architecture and Gardens* 3, 58-64.
- Liu, D. K. (2001b). "Load assembler of roofing of ancient building (The second volume)," *Traditional Chinese Architecture and Gardens* 4, 56-63.
- Li, S., Zhou, Z., Luo, H., Milani, G., and Abruzzese, D. (2020). "Behavior of traditional Chinese mortise-tenon joints: Experimental and numerical insight for coupled vertical and reversed cyclic horizontal loads," *Journal of Building Engineering* 30, article 101257. DOI: 10.1016/j.job.2020.101257
- Li, Y. Z. (2015). *Experimental Study on Seismic Behavior of Dovetail Mortise-tenon Joints under Different Loose Degrees in Ancient Timber Buildings*, Master's Thesis, Xi'an University of Architecture and Technology, Xi'an, China.
- Ma, B. J. (2003) *Wooden Construction Technology of Ancient Chinese Architecture*, Science Press: Beijing, China.
- Maeno, M., Suzuki, Y., Ohshita, T., and Kitahara, O. (2004). "Seismic response characteristic of traditional wooden frame by full-scale dynamic and static tests," in: *13<sup>th</sup> World Conference on Earthquake Engineering*, Vancouver, B.C., Canada. No. 1184.
- Meng, X. J., Li, T. Y., and Yang, Q. S. (2019). "Experimental study on the seismic mechanism of a full-scale traditional Chinese timber structure," *Engineering Structures* 180, 484-493 DOI: 10.1016/j.engstruct.2018.11.055
- Pan, Y., An, R. B., Wang, X. Y., and Guo, R. (2020). "Study on mechanical model of through-tenon joints in ancient timber structures," *China Civil Engineering Journal* 53(4), 61-70, 82. DOI:10.15951/j.tmgcxb.2020.04.007
- Pan, Y., Zhang, Q. Wang, X. Y., and Guo, R. (2021). "Research on mechanical model of dovetail joint for Chinese ancient timber structures," *Journal of Building Structures* 42(8), 151-159. DOI: 10.14006 /j. jzjgxb. 2019. 0528
- Sun, G. J., Zhao, Y. F., Xue, S. D., and Li, J. (2020). "Pseudo-static experimental study on composite mortise-tenon joint composed of king post and ridge purlin of Chinese timber beam frame structure of Qing Dynasty," *Building Structure* 50(16), 82-86.

- DOI: 10.19701/j.jzjg.2020.16.014.
- Sun, Z., Xiang, P., Jia, L., and Zhang, R. (2022). “Seismic response and kinematic mechanisms of single-story pavilion-type timber frame based on shaking table test,” *Structures* 2022, 45, 1701-1716. DOI: 10.1016/j.istruc.2022.10.016.
- Wan, J., Yang, Q., Wei, J., and Li, T. (2020). “Initial motion analysis of traditional Chinese rocking timber frame subjected to horizontal ground motion: Theoretical and numerical investigations,” *Engineering Structures* 203, article 109898. DOI: 10.1016/j.engstruct.2019.109898
- Wang, J., Cui, Z., Yu, L., Xu, R., and Yang, Q. (2022). “Analysis of the seismic behavior of traditional Chinese timber structures in the Tang dynasty,” *Structures* 41, 447-462. DOI: 10.1016/j.istruc.2022.05.007.
- Wang, J., Xu, R. W., Zhang, X. M., and Yang, Q. S. (2021). “Parameter analysis on lateral force resistance of the palace-style timber structure in Tang Dynasty,” *Journal of Civil and Environmental Engineering* 44(02), 48-59. DOI: 10.11835/j.issn.2096-6717.2021.020
- Wu, Y. J., Lin, H. T., Xie, Q. F., Wang, L., and Zhang, L. P. (2022). “Lateral performance of columns in ancient timber structures considering the influence of Pu-pai Fang,” *Journal of Building Structures* 1-12. DOI:10.14006/j.jzjgxb.2022.0493.
- Xie, Q. F., Zhang, L. P., Xiang, W., and Qian, C. Y. (2018). “Experimental study and finite element analysis of Dou Gong joints built with fork column under vertical loading,” *Journal of Building Structures* 39(9), 66-74. DOI: 10.14006/j.jzjgxb.2018.09.008
- Zhou, Q., and Yan, W. M. (2012). “Bending analysis on composite beam and combination beam of Chinese ancient wooden buildings,” *Building Structure* 42(4), 157-161. DOI: 10.19701/j.jzjg.2012.04.033.
- Zhou, Q., and Yang, N. (2016). “Typical structural health problems of purlin components of ancient buildings in the Forbidden City,” *Journal of Water Resources and Architectural Engineering* 14(5), 61-69, 169. DOI: 10.3969/j.issn.1672-1144.2016.05.012.

Article submitted: April 19, 2023; Peer review completed: May 7, 2023; Revised version received and accepted: May 9, 2023; Published: May 19, 2023.

DOI: 10.15376/biores.18.3.4723-4738